Enhanced Channel Estimation for RIS-assisted OTFS Systems by Introducing ELM Network

Chaojin Qing[1,*], Zhiying Liu[1], Li Wang[1], Guowei Ling[1], Wenquan Hu[1], Xi Cai[1], and Hui Lin[2]

[1]School of Electrical Engineering and Electronic Information, Xihua University, Chengdu, 610039, China
[2]Chengdu Aerospace Kate Electromechanical Technology Co., Ltd., Chengdu, 611730, China
[*]qingchj@mail.xhu.edu.cn

ABSTRACT

In high-mobility communication scenarios, leveraging reconfigurable intelligent surfaces (RIS) to assist orthogonal time frequency space (OTFS) systems proves advantageous. However, the integration of RIS into OTFS systems has added complexity to the channel estimation (CE). Utilizing the benefits of machine learning (ML) to address such intricate issues holds the potential to reduce the complexity of CE. Yet, there is a lack of investigations of ML-based CE in RIS-assisted OTFS systems, leaving significant blanks and posing challenges for intelligent applications. Additionally, ML-based CE still faces numerous difficulties, such as intricate parameter tuning and long training time. Inspired by the inherent advantages of the single-hidden layer feed-forward network structure, we introduce extreme learning machine (ELM) into RIS-assisted OTFS systems to improve their CE accuracy. In this method, we integrate a threshold-based approach to extract initial feature, aiming to remedy the inherent limitations of ELM network, such as inadequate network parameters compared to the deep learning network. This initial feature is then leveraged to enhance ELM learning ability, leading to improved CE accuracy. By using the classic message passing algorithm to detect data symbols, simulation results demonstrate that the proposed method efficiently improves the symbol detection (SD) performance of RIS-assisted OTFS systems. Furthermore, the SD performance is robust against the impacts of the parameter variations.

I. Introduction

The key performance requirements in next generation wireless communication contain high-mobility, increased energy and spectral efficiency, high reliability and low latency[1]. In high-mobility communication scenarios, orthogonal time frequency space (OTFS) modulation has been widely considered[2–5] to ensure the reliability. However, communication interruptions frequently occur as a result of physical blockages in wireless scenarios[6]. Reconfigurable intelligent surfaces (RIS)[7–9] emerge as a highly promising technology to tackle this issue. Therefore, a combination of RIS and OTFS offers comprehensive advantages, including flexile channel configuration and reliable communication in high-mobility scenarios.

Channel estimation (CE) plays a crucial role in the receiver design. In recent years, CE methods for OTFS systems have been widely investigated[3,4], providing potential insights for the CE in RIS-assisted OTFS systems. Moreover, recent studies have investigated that the deployment of RIS in OTFS systems can effectively enhance OTFS performance. In[10], it is demonstrated that RIS-assisted OTFS systems outperform RIS-assisted OFDM systems, and exhibit excellent performance over a wide range of channel parameters. An efficient and reliable transmission scheme is proposed in[11], which leverages the information in the delay-Doppler (DD) domain to facilitate the configuration of RIS. In[12], a joint CE and symbol detection (SD) method for hybrid RIS-assisted millimeter wave OTFS systems is presented. The proposed method combines the expectation maximization algorithm with the message passing (MP) algorithm to estimate the wireless channel and detect the data symbols. While RIS-assisted OTFS systems have achieved significant performance advantages[10–12], the introduction of RIS inevitably increases the complexity of CE in OTFS systems. The large number of passive reflective elements from RIS results in a tremendously large channel matrix dimension[13]. Additionally, the lack of signal processing capability in the passive components of RIS exacerbates the processing complexity[14].

Leveraging the significant advantages of machine learning (ML) in addressing complex problems, the introduction of ML into RIS-assisted OTFS systems holds the promise of overcoming their CE challenges. It is evidenced that ML, in particular deep learning (DL) improves communication system performance by learning from the wireless networking environment, allowing for adaptive network optimization[15]. Notably, preliminary endeavors have been undertaken to investigate the design of RIS-assisted OTFS systems by incorporating ML. For example, a DL-based signal detector is proposed for the RIS-aided OTFS systems in[16], and it achieves a significant improvement in bit-error-rate (BER) performance. However, there are few studies focusing on ML-based CE for RIS-assisted OTFS systems.

To fill in this blank, introducing ML into the CE of RIS-assisted OTFS systems is a highly promising solution. However, among numerous ML methods, DL-based approaches face challenges such as intricate parameter tuning, extensive dataset collection, and prolonged training times, etc[17]. In contrast, extreme learning machine (ELM)-based methods exhibit significant advantages, making them an attractive potential solution[18]. Unlike DL-based approaches, the ELM benefits from its single-hidden layer feed-forward neural network structure[18]. This key feature obviates the need for gradient back-propagation (BP) and confers several notable advantages, such as exceptional learning speed (hundreds of times faster than the BP algorithm) and impressive generalization performance[19–21].

Inspired by the advantages of the ELM network, this paper introduces ELM into the CE of RIS-assisted OTFS systems to enhance estimation accuracy. Specifically, recognizing the inherent limitations of ELM, e.g., the inadequate network parameters relative to the DL network, we integrate a threshold-based method to extract initial feature. Then, we develop an ELM network to improve CE accuracy according to the extracted initial feature. Leveraging the enhanced channel state information, we recover data symbols by using the classic MP algorithm[22]. The proposed method efficiently facilitates CE for high-mobility communication scenarios, thereby benefiting the subsequent SD with the enhanced CE. Our simulation results demonstrate the method's robustness against modulation order and user speed impacts. The main contributions of this paper are as follows:

- We propose an enhanced CE method for RIS-assisted OTFS systems by introducing an ELM network. To the best of our knowledge, there is no existing works investigating the ML-based CE for RIS-assisted OTFS systems. Our work fills this gap. In particular, we introduce ELM networks to alleviate challenges faced in DL-based CE, such as intricate parameter tuning and long training time.
- We integrate a threshold-based initial feature extraction method tailored to overcome the limited learning capacity of ELM networks compared to DL networks, attributed to their insufficient network parameters. This initial feature extraction takes into account the specificity of CE in OTFS systems, setting it apart from current ELM-based CE methods (e.g.,[19]).
- We incorporate the cascaded channels of RIS into the representation of the DD domain equivalent channel of the OTFS systems. This enables the simplification of CE in high-mobility communication scenarios by leveraging the approximately time-invariant channel characteristics in the DD domain[23], and thus improves the CE accuracy of RIS-assisted OTFS systems[12].

The rest of this paper is organized as follows. Section II illustrates the system model of RIS-assisted OTFS. In Section III, an enhanced CE method by introducing ELM network is proposed. Section IV provides numerical simulation results and performance analysis. Finally, we conclude the paper in Section V.

Notations: Bold face lower case and upper case letters represent vector and matrix, respectively. $(\cdot)^{\mathrm{T}}$ and $(\cdot)^{\mathrm{H}}$ denote the transpose and conjugate transpose, respectively. $\odot$ and $\otimes$ stands for the Hadamard product and Kronecker product, respectively. $\mathbf{F}_{\alpha}$ $(\alpha = M, N)$ is the normalized $\alpha \times \alpha$ Fourier transform matrix. $\mathrm{vec}(\cdot)$ and $\mathrm{vec}^{-1}(\cdot)$ denote the column vectorization and its inverse operation, respectively. $\mathbf{I}_M$ stands the M-order unit matrix.

II. System Model

As shown in Fig. 1, the RIS-assisted OTFS systems with N delay and M Doppler bins is considered in this paper. At the transmitter (TX), the information bits are mapped to DD grids to form $\mathbf{X}_{\mathrm{DD}} \in \mathbb{C}^{M \times N}$. By using the inverse symplectic finite fourier transform (ISFFT), $\mathbf{X}_{\mathrm{DD}}$ is transformed to the time-frequency (TF) domain, which is expressed as[24]

$$\mathbf{X}_{\mathrm{TF}} = \mathbf{F}_M \mathbf{X}_{\mathrm{DD}} \mathbf{F}_N^{\mathrm{H}}, \tag{1}$$

where $\mathbf{X}_{\mathrm{TF}} \in \mathbb{C}^{M \times N}$ denotes the TF domain variant of $\mathbf{X}_{\mathrm{DD}}$. The Heisenberg transform is employed to transform the TF signal $\mathbf{X}_{\mathrm{TF}}$ to the time domain (TD) signal $\mathbf{S} \in \mathbb{C}^{M \times N}$, i.e.,

$$\mathbf{S} = \mathbf{G}_{\mathrm{tx}} \mathbf{F}_M^{\mathrm{H}} \mathbf{X}_{\mathrm{TF}}, \tag{2}$$

where $\mathbf{G}_{\mathrm{tx}} \in \mathbb{C}^{M \times M}$ denotes the pulse-shaping matrix[24]. From[24] and[25], $\mathbf{G}_{\mathrm{tx}}$ is a diagonal matrix and its diagonal entries are sampled from the pulse-shaping waveform. For the rectangular waveform, $\mathbf{G}_{\mathrm{tx}}$ reduces to the identity matrix (i.e., $\mathbf{G}_{\mathrm{tx}} = \mathbf{I}_M$)[24,25], and Eq. (2) can be rewritten as

$$\mathbf{S} = \mathbf{F}_M^{\mathrm{H}} \mathbf{X}_{\mathrm{TF}}. \tag{3}$$

According to the column-wise vectoring, the TD vector signal $\mathbf{s} \in \mathbb{C}^{MN \times 1}$ is given by

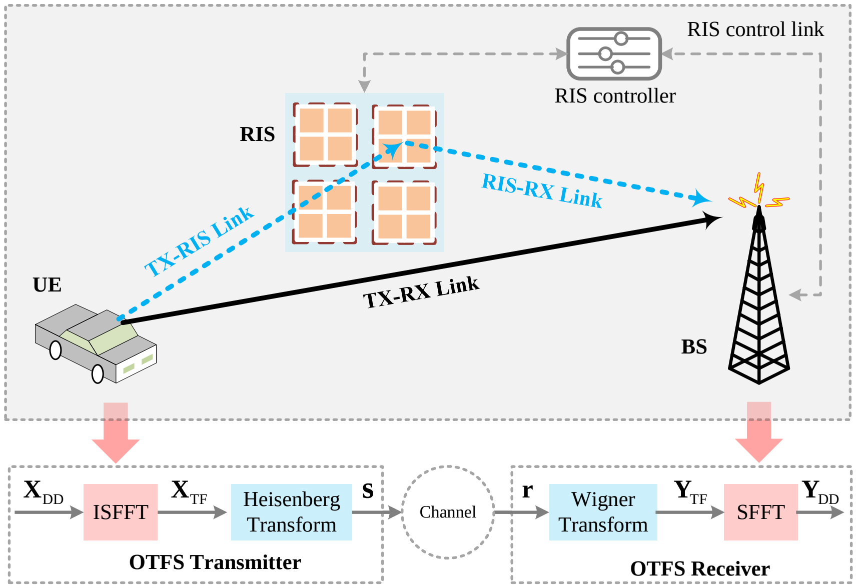

Figure 1. RIS-assisted OTFS systems.

$$\mathbf{s} = \mathrm{vec}\left(\mathbf{S}\right). \tag{4}$$

After appending a cyclic prefix (CP), the TD signal is transmitted to the receiver (RX) over the wireless channels.

From[19], we consider the RIS-assisted systems with R sub-surfaces to reflect P resolvable paths. The composite channel impulse responses (CIRs) between the TX and RX, denoted as $\mathbf{h} \in \mathbb{C}^{P\times 1}$, is given by[19]

$$\mathbf{h} = \mathbf{h}_{\mathrm{TR}} + \mathbf{h}_{\mathrm{TRR}}\phi, \tag{5}$$

where $\mathbf{h}_{\mathrm{TR}} \in \mathbb{C}^{P\times 1}$ denotes the CIRs of the direct TX-RX link, $\mathbf{h}_{\mathrm{TRR}} \in \mathbb{C}^{P\times R}$ stands the equivalent cascaded CIRs of the reflecting link (i.e., TX-RIS-RX link), and $\phi \in \mathbb{C}^{R\times 1}$ is the phase-shift vector of R sub-surfaces. From[19], we express $\mathbf{h}_{\mathrm{TRR}}$ and ϕ as

$$\mathbf{h}_{\mathrm{TRR}} = [\mathbf{h}_{\mathrm{TRR},1}, \mathbf{h}_{\mathrm{TRR},2}, \cdots \mathbf{h}_{\mathrm{TRR},R}], \tag{6}$$

and

$$\phi \triangleq [\phi_1, \phi_2, \cdots, \phi_R]^{\mathrm{T}}, \tag{7}$$

where $\mathbf{h}_{\mathrm{TRR},r} \in \mathbb{C}^{P\times 1}$ and $\phi_r = \alpha_r e^{j\varphi_r}$ with $r = 1, \cdots, R$ denote the equivalent cascaded CIRs and the phase-shift vector of the r-th sub-surface, respectively. In this paper, $\alpha_r = 1$ and $\varphi_r \in [0, 2\pi]$ are considered to maximize the reflection power and simplify hardware implementation[26]. For the r-th sub-surface, the equivalent cascaded channel $\mathbf{h}_{\mathrm{TRR},r}$ is given by

$$\mathbf{h}_{\mathrm{TRR},r} = \mathbf{h}_{\mathrm{TRS},r} \odot \mathbf{h}_{\mathrm{RSR},r}, \tag{8}$$

where $\mathbf{h}_{\mathrm{TRS},r} \in \mathbb{C}^{P\times 1}$ and $\mathbf{h}_{\mathrm{RSR},r} \in \mathbb{C}^{P\times 1}$ are the equivalent CIRs of the TX-RIS link and RIS-RX link corresponding to the r-th sub-surface, respectively.

According to Eq. (5) and Eq. (8), the composite channel $\mathbf{h}$ can be rewritten as

$$\mathbf{h} = \mathbf{h}_{\mathrm{TR}} + \sum_{r=1}^{R} \left(\mathbf{h}_{\mathrm{TRS},r} \odot \mathbf{h}_{\mathrm{RSR},r}\phi_r\right). \tag{9}$$

For P resolvable paths, we have

$$\mathbf{h} = [h_1, h_2, \cdots, h_P]^{\mathrm{T}}. \tag{10}$$

Then, the transmission channel $\mathbf{H} \in \mathbb{C}^{MN \times MN}$ can be represented as[24]

$$\mathbf{H} = \sum_{p=1}^{P} h_p \Pi^{l_p} \Delta^{k_p}, \tag{11}$$

where h_p with $p = 1, \cdots, P$ is the p-th entry of $\mathbf{h}$, Π is the $MN \times MN$ permutation matrix (forward cyclic shift), Δ represents the $MN \times MN$ diagonal matrix, and l_p and k_p are the delay and Doppler taps of the p-th path on the DD grid, respectively. From[3], we have $l_p = (M\Delta f)\tau_p$ and $k_p = (NT)\upsilon_p$, where Δf, τ_p, T and υ_p denote the subcarrier interval, the p-th path delay, the sampling interval, and the Doppler shift of the p-th path, respectively.

After removing the CP at the receiver, the received TD signal $\mathbf{r} \in \mathbb{C}^{MN \times 1}$ is given by[24]

$$\mathbf{r} = \mathbf{H}\mathbf{s} + \mathbf{n}, \tag{12}$$

where $\mathbf{n} \in \mathbb{C}^{MN \times 1}$ denotes the complex additive white Gaussian noise vector satisfying $\mathbf{n} \sim \mathcal{CN}(\mathbf{0}, \sigma^2 \mathbf{I}_{MN})$. By using the Wigner transform, the TD signal $\mathbf{r}$ is mapped to the TF domain to form $\mathbf{Y}_{\mathrm{TF}} \in \mathbb{C}^{M \times N}$, which can be expressed as[27]

$$\mathbf{Y}_{\mathrm{TF}} = \mathbf{F}_M \cdot \mathbf{G}_{\mathrm{rx}} \cdot \mathrm{vec}^{-1}(\mathbf{r}), \tag{13}$$

where $\mathbf{G}_{\mathrm{rx}} \in \mathbb{C}^{M \times M}$ stands the pulse-shaping matrix at the receiver. In this paper, $\mathbf{G}_{\mathrm{rx}} = \mathbf{I}_M$ is considered for rectangular pulse shaping[27].

By using symplectic finite fourier transform (SFFT), $\mathbf{Y}_{\mathrm{TF}}$ is transformed to the DD domain to form $\mathbf{Y}_{\mathrm{DD}} \in \mathbb{C}^{M \times N}$, which is expressed as[27]

$$\mathbf{Y}_{\mathrm{DD}} = \mathbf{F}_M^{\mathrm{H}} \cdot \mathbf{Y}_{\mathrm{TF}} \cdot \mathbf{F}_N. \tag{14}$$

With the DD domain signal $\mathbf{Y}_{\mathrm{DD}}$, an enhanced CE method by introducing the ELM network is proposed in Section III to improve the CE accuracy for RIS-assisted OTFS systems.

III. Enhanced CE by Introducing ELM Network

In this section, the proposed enhanced CE for RIS-assisted OTFS systems using the ELM network is elaborated. In Section III-A, the pilot deployment in the DD domain is given. Then, the initial feature extraction, which is employed to enhance ELM learning, is presented in Section III-B. With the extracted initial feature, an ELM-enhanced CE (ELM-EnCE) scheme is developed in Section III-C.

A. Pilot Placement

The pilot placement scheme in[3] is employed to assist the CE in RIS-assisted OTFS systems. From[3], a single pilot symbol is embedded in the DD grids, which is guarded by zero-valued symbol for each OTFS transmission frame in the DD domain (i.e., $\mathbf{X}_{\mathrm{DD}}$). The symbol placement diagram is shown in Fig. 2(a), where the pilot location is indexed by $[k_{\mathrm{pilot}}, l_{\mathrm{pilot}}]$ with $0 \le k_{\mathrm{pilot}} \le N-1$ and $0 \le l_{\mathrm{pilot}} \le M-1$. Then, the transmitted symbol (i.e., the pilot symbol, guard symbols, and data symbols) on the (k,l)-th DD grid is given by[3]

$$x[k,l] = \begin{cases} x_{\mathrm{pilot}}, & k = k_{\mathrm{pilot}} \text{ and } l = l_{\mathrm{pilot}} \\ 0, & k_{\mathrm{pilot}} - 2k_\nu \le k \le k_{\mathrm{pilot}} + 2k_\nu \\ & \text{and } l_{\mathrm{pilot}} - l_\tau \le l \le l_{\mathrm{pilot}} + l_\tau \\ x_{\mathrm{d}}[k,l], & \text{otherwise} \end{cases}, \tag{15}$$

where x_{pilot}, $x_{\mathrm{d}}[k,l]$, l_τ and k_ν denote the pilot symbol, the (k,l)-th data symbol, the maximum delay tap and the maximum Doppler tap, respectively. It is important to note that pilot placement scheme in[3] is merely considered as an example in this paper, and other methods of pilot placement can also be employed for the CE of this paper.

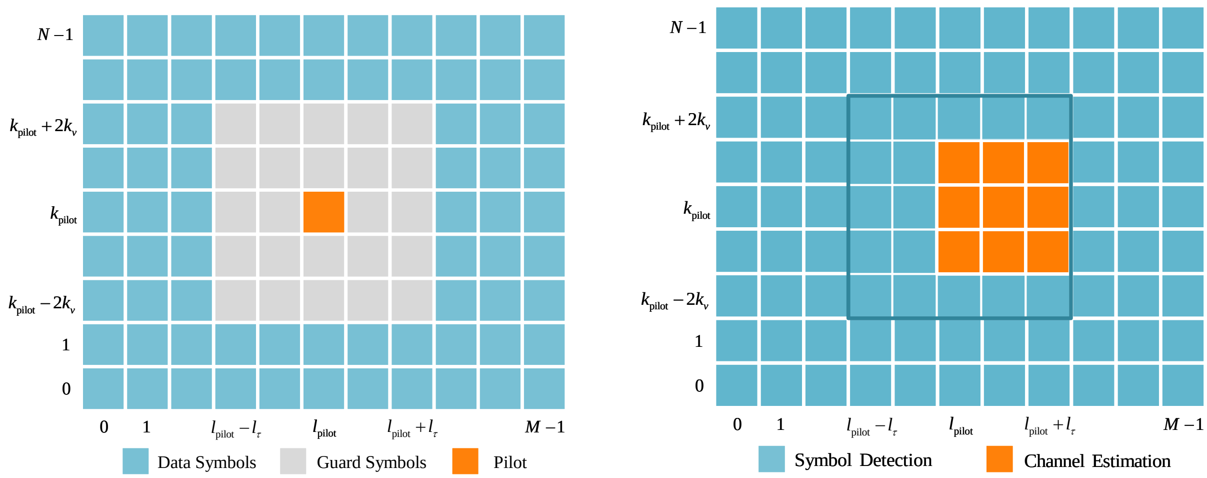

(a) Symbol placement diagram at the transmitter.

(b) The schematic diagram of received symbols.

Figure 2. The schematic diagram of the symbols at transceiver[3].

B. Initial Feature Extraction

Based on the pilot placement scheme in[3], the threshold-based method in[28] is utilized for the CE in this paper. The schematic diagram of the received signal $\mathbf{Y}_{\mathrm{DD}}$ is shown in Fig. 2(b), where the entry $y_{\mathrm{DD}}[k,l]$ with $k_{\mathrm{pilot}} - k_\upsilon \le k \le k_{\mathrm{pilot}} + k_\upsilon$ and $l_{\mathrm{pilot}} \le l \le l_{\mathrm{pilot}} + l_\tau$ is used to detect the resolvable paths, and the remaining symbols on the grid are used for SD. For the given positive threshold T_h, we assume that there exist P distinguishable paths in this paper. By denoting the index of the p-th distinguishable path on the DD grids as $\left(\widetilde{k}_p, \widetilde{l}_p\right)$, its path gain is estimated as

$$\widehat{h}_{\mathrm{DD}}\left[\widetilde{k}_p,\widetilde{l}_p\right] = \frac{y_{\mathrm{DD}}\left[\widetilde{k}_p,\widetilde{l}_p\right]}{x_{\mathrm{pilot}}}, \text{ if } \left|y_{\mathrm{DD}}\left[\widetilde{k}_p,\widetilde{l}_p\right]\right| \ge T_h. \tag{16}$$

With the estimated $\widehat{h}_{\mathrm{DD}}\left[\widetilde{k}_p,\widetilde{l}_p\right]$ in Eq. (16), the equivalent channel in the DD domain, denoted as $\widehat{\mathbf{H}} \in \mathbb{C}^{MN\times MN}$, is given by[24]

$$\widehat{\mathbf{H}} = \sum_{p=1}^{P} \widehat{h}_{\mathrm{DD}}\left[\widetilde{k}_p,\widetilde{l}_p\right] \Pi^{\widetilde{l}_p} \Delta^{\widetilde{k}_p}. \tag{17}$$

Usually, the threshold-based CE encounters noise and interference, degrading the CE accuracy[29]. To address this issue, we view $\widehat{\mathbf{H}}$ as the initial feature (or coarse estimation) in this paper and introduce an ELM network to improve the CE accuracy. In an ELM network, the vectorized input is usually required. Thus, the initial feature of the ELM network (denoted as $\widetilde{\mathbf{H}} \in \mathbb{C}^{M^2N^2\times 1}$) can be obtained by vectoring $\widehat{\mathbf{H}}$ column-wise, i.e.,

$$\widetilde{\mathbf{H}} = \mathrm{vec}\left(\widehat{\mathbf{H}}\right). \tag{18}$$

With the initial feature $\widetilde{\mathbf{H}}$, we design an ELM network in Section III-C to enhance the CE accuracy.

***Remark 1**: By integrating the cascaded channel $\mathbf{h}_{\mathrm{TRR}}$ of RIS system into the equivalent channel $\mathbf{H}$ of the DD domain in OTFS system, the time-varying wireless channel transforms into a quasi-static wireless channel. This proves beneficial for CE in high-speed mobile communication scenarios. Consequently, based on the pilot placement scheme of[3], the threshold-based CE method in[28] effectively estimate the quasi-static channel, extracting significant channel features.*

C. CE Enhancement with ELM Network

The developed ELM network is presented in **Algorithm 1** and its main phases are described as follows.

Network Architecture

The number of the input and output neurons is designed as M^2N^2 to ensure consistency with the data dimension, and the hidden neurons are configured as $2M^2N^2$ to effectively capture the input feature. From[19], the sigmoid function is employed as the activation function, which is defined as $\sigma(x) = 1/(1+e^{-x})$. The input weights $\mathbf{W} \in \mathbb{C}^{2M^2N^2 \times M^2N^2}$ and biases $\mathbf{b} \in \mathbb{C}^{2M^2N^2 \times 1}$ are randomly initialized for ELM training[19]. With the designed network architecture, the ELM network learns the output weight matrix by offline training.

Algorithm 1: The algorithm of ELM-EnCE

Input: The received signal $\mathbf{Y}_{\mathrm{DD}}$, the input weights $\mathbf{W}$ and biases $\mathbf{b}$ of the ELM, and the number of training samples, i.e., Q.

Output: The output weight of the hidden layer (i.e., $\boldsymbol{\Upsilon}$), and the enhanced CE $\mathbf{H}_{\mathrm{en}}$.

Offline training:

for $q = 1, \cdots, Q$ **do**

  Collect the q-th training sample $\widetilde{\mathbf{H}}_q$ according to the equations from Eq. (16) to Eq. (18).

  Calculate the hidden layer output $\mathbf{o}_q$ according to Eq. (19).

end

Collect $\mathbf{o}_1, \cdots, \mathbf{o}_Q$ to form $\mathbf{O} = [\mathbf{o}_1, \cdots, \mathbf{o}_Q]$, i.e., Eq. (20).

Calculate the output weight of the hidden layer (i.e., $\boldsymbol{\Upsilon}$) by using Eq. (21).

Online deployment:

By using Eq. (13) and Eq. (14), we transform the received $\mathbf{r}$ to the DD domain to obtain $\mathbf{Y}_{\mathrm{DD}}$.

Estimate $\widehat{h}_{\mathrm{DD}}\left[\widetilde{k}_p, \widetilde{l}_p\right]$ (i.e., the gain of the p-th path) according to Eq. (16), i.e., the threshold-based estimation method.

Estimate the equivalent channel $\widehat{\mathbf{H}}$ in the DD domain by using Eq. (17).

Vectorize $\widehat{\mathbf{H}}$ column-wise to obtain the initial feature matrix $\widetilde{\mathbf{H}}$ according to Eq. (18).

Feed $\widetilde{\mathbf{H}}$ into the trained ELM network to obtain the enhanced CE $\mathbf{H}_{\mathrm{en}}$.

Offline Training

The training dataset consists of Q samples, which is denoted as $\left\{\left(\widetilde{\mathbf{H}}_q, \widetilde{\mathbf{H}}_{\mathrm{Label},q}\right), q = 1, 2, \cdots, Q\right\}$ with $\widetilde{\mathbf{H}}_q$ and $\widetilde{\mathbf{H}}_{\mathrm{Label},q}$ being the training data and training label of the q-th sample, respectively. The training set of the ELM is generated through Eq. (16) to Eq. (18). In this paper, the number of training samples is set as $Q = 10^4$[19]. With the q-th training sample $\left(\widetilde{\mathbf{H}}_q, \widetilde{\mathbf{H}}_{\mathrm{Label},q}\right)$, the hidden layer output, denoted as $\mathbf{o}_q \in \mathbb{C}^{2M^2N^2 \times 1}$, is calculated by

$$\mathbf{o}_q = \sigma\left(\mathbf{W}\widetilde{\mathbf{H}}_q + \mathbf{b}\right). \tag{19}$$

By collecting $\mathbf{o}_1, \cdots, \mathbf{o}_Q$, we have

$$\mathbf{O} = [\mathbf{o}_1, \cdots, \mathbf{o}_Q], \tag{20}$$

where $\mathbf{O} \in \mathbb{C}^{2M^2N^2 \times Q}$ is employed to form the output weight matrix of the hidden layer. By denoting this output weight matrix as $\boldsymbol{\Upsilon} \in \mathbb{C}^{M^2N^2 \times 2M^2N^2}$, then we have[19]

$$\boldsymbol{\Upsilon} = \widetilde{\mathbf{H}}_{\mathrm{Label}}\mathbf{O}^{\mathrm{H}}, \tag{21}$$

where $\widetilde{\mathbf{H}}_{\mathrm{Label}} = [\widetilde{\mathbf{H}}_{\mathrm{Label},1}, \widetilde{\mathbf{H}}_{\mathrm{Label},2}, \cdots, \widetilde{\mathbf{H}}_{\mathrm{Label},Q}]$ with $\widetilde{\mathbf{H}}_{\mathrm{Label}} \in \mathbb{C}^{M^2N^2 \times Q}$.

Online Deployment

According to Eq. (13) and Eq. (14), the received $\mathbf{r}$ given in Eq. (12) is transformed to the DD domain to obtain $\mathbf{Y}_{\mathrm{DD}}$. By using the threshold-based estimation, the path gain $\widehat{h}_{\mathrm{DD}}\left[\widetilde{k}_p, \widetilde{l}_p\right]$ is obtained according to Eq. (16). Then, the DD domain equivalent channel matrix $\widehat{\mathbf{H}}$ is generated according to Eq.(17). By using Eq. (18), the generated $\widehat{\mathbf{H}}$ is vectorized column-wise to form

$\widetilde{\mathbf{H}}$. Finally, we view $\widetilde{\mathbf{H}}$ as the initial network feature and use the ELM network to enhance the CE. By denoting the enhanced estimation as $\mathbf{H}_{\text{en}} \in \mathbb{C}^{M^2N^2 \times 1}$, we have

$$\mathbf{H}_{\text{en}} = \boldsymbol{\Upsilon} \cdot \sigma \left(\mathbf{W}\widetilde{\mathbf{H}} + \mathbf{b} \right). \tag{22}$$

With the enhanced CE (i.e., $\mathbf{H}_{\text{en}}$), the SD algorithm (e.g., MP algorithm in[22]) is employed to recover the data symbol, which benefits from the enhanced CE as well.

***Remark 2**: The threshold-based CE method presented in[28] dose not consider the denoising processing, degrading the CE accuracy. This inaccuracy of CE declines subsequent SD performance. Therefore, the ELM network developed in this paper can be viewed as a denoising network. The initial feature extraction and CE enhancement with the ELM network mutually complement each other. On one hand, the single hidden layer of ELM network structure imposes limitations on its learning ability. Leveraging the threshold-based feature extraction in[28] as the preprocessing facilitates ELM learning by focusing solely on denoising significant path features. On the other hand, the threshold-based channel estimation from[28] also benefits from the denoising capabilities of ELM network. With offline training, the ELM captures noise and interference distributions, providing valuable statistical insights to enhance the estimation accuracy of the complex gains on significant paths.*

IV. Results and Discussions

In this section, we validate the effectiveness and robustness of the proposed CE method by numerical simulations. In Section IV-A, the basic parameters involved in the simulations are given. Then, we verify the effectiveness of ELM-EnCE for RIS-assisted OTFS systems in Section IV-B. The robustness analysis against parameter impacts is presented in Section IV-C.

A. Parameters Settings

The basic parameters involved in the simulations are given as follows. $M = 16$, $N = 8$, and $R = 8$[19,30]. From[3], the carrier frequency f_c, the subcarrier interval Δf, and the data modulation are set as 4 GHz, 15 kHz, and 4-quadrature amplitude modulation (4-QAM), respectively. We employ the standard Extended Vehicular A model with a speed of 300 km/h as the wireless channel model[31]. The Doppler shift corresponding to the p-th tap is generated by Jake's spectrum and is defined as $v_p = v_{\max}\cos(\varphi_p)$, where $v_{\max}$ is the maximum Doppler shift with 1.1×10^3 Hz and φ_p is uniformly distributed over $[0, 2\pi]$. For data detection, the MP algorithm in[22] is utilized and the number of iterations is set to 15. The given ELM network is trained and tested on an Intel Xeon(R) E5-2620 CPU 2.1GHz 16 server.

For expression simplicity, we utilize "Ref[4]", "RIS-OTFS-MP" and "Prop" to represent the comparison method from[4], the proposed method without introducing ELM, and the proposed ELM-EnCE method for RIS-assisted OTFS systems, respectively.

B. Effectiveness Analysis

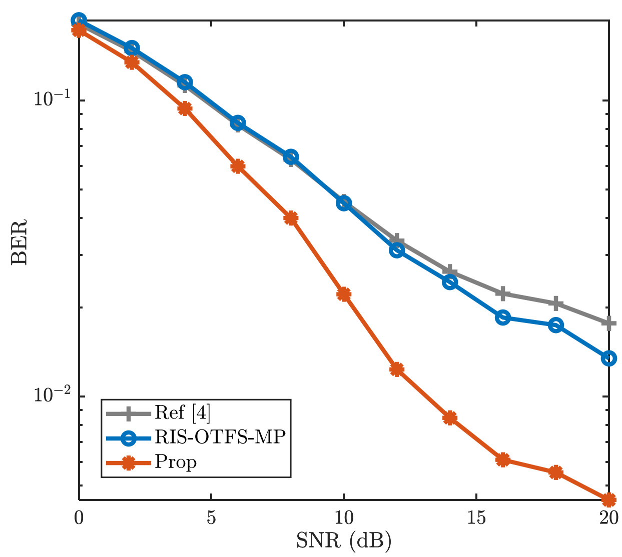

Figure 3. BER vs. SNR, where the methods of "Ref[4]", "RIS-OTFS-MP", and "Prop" are compared.

To validate the effectiveness of the proposed method, Fig. 3 shows the BER performance. From Fig. 3, the BER of "Prop" is lower than those of "Ref[4]" and "RIS-OTFS-MP" for each simulated SNR. For example, when SNR is 20 dB, the "Prop" achieves a BER of 4.4×10^{-3}, while the BERs of "Ref[4]" and "RIS-OTFS-MP" are both larger than 10^{-2}. This indicates that the "Prop" is effective to improve the CE accuracy of "RIS-OTFS-MP" and "Ref[4]", and thus reducing their BERs. Notably, the BER of "Prop" is lower than that of "RIS-OTFS-MP" for each given SNR. This validates the effectiveness of introducing the ELM network, i.e., the proposed ELM-EnCE effectively enhances the BER performance of "RIS-OTFS-MP". Without introducing the ELM network, "RIS-OTFS-MP" only slightly improves the BER of "Ref[4]" in relatively high SNR regions, e.g., SNR larger than 14 dB. In conclusion, the proposed method is effective in improving the CE performance of "Ref[4]", particularly with the introduction of the ELM network.

C. Robustness Analysis

In this subsection, the robustness of the proposed method against the impacts of the modulation order I (of QAM) and the user speed v is discussed. With the exception of the parameters discussed in the robustness analysis, other basic parameters remain the same as those detailed in Section IV-A.

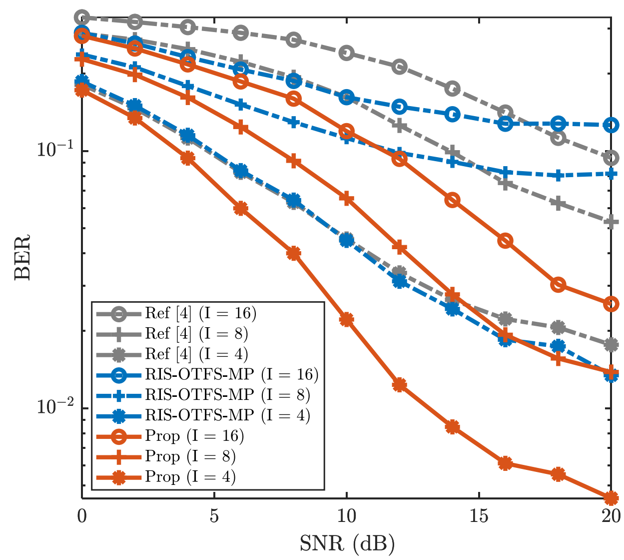

Figure 4. BER vs. SNR, where $I = 4$, $I = 8$ and $I = 16$ are considered.

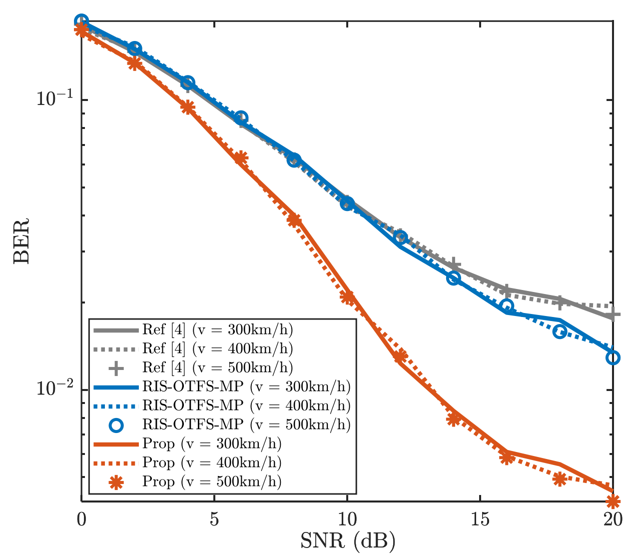

Figure 5. BER vs. SNR, where $v = 300$ km/h, $v = 400$ km/h and $v = 500$ km/h are considered.

Robustness against I

In Fig. 4, we illustrate the robustness of the proposed method against the impact of the modulation order I, where $I = 4$, $I = 8$ and $I = 16$ are considered. From Fig. 4, it is evident that BERs increase as the modulation order I increases. For example, when SNR is 10 dB, the "Prop" with 4-QAM performs a BER of 4×10^{-2}, while the BERs of 8-QAM and 16-QAM are about 8.5×10^{-2} and larger than 10^{-1}, respectively. Furthermore, Fig. 4 shows that the "Prop" achieves a lower BER than those of "Ref[4]" and "RIS-OTFS-MP" for each given value of modulation order I. With 4-QAM, when SNR is 20 dB, the BER of "Prop" is about 4×10^{-3}, while the BERs of "Ref[4]" and "RIS-OTFS-MP" are both larger than 10^{-2}. Against the varying of modulation order I, the BER performance of the proposed method is still better than those of "Ref[4]" and "RIS-OTFS-MP". Thus, the proposed method possesses a good robustness against the impact of the modulation order I.

Robustness against v

Fig. 5 presents the robustness of the proposed method under different user speeds (i.e., $v = 300$ km/h, $v = 400$ km/h and $v = 500$ km/h). The "Prop" exhibits resemble BERs under different user speeds. For example, when SNR is 20 dB, the BERs of "Prop" under different v are all about 4.5×10^{-3}. Besides, from Fig. 5, it can be seen that the "Prop" achieves the lower BER than those of "Ref[4]" and "RIS-OTFS-MP". As the SNR is 20 dB, the BER of "Prop" is about 4.5×10^{-3}, while the BERs of "Ref[4]" and "RIS-OTFS-MP" are both larger than 10^{-2}. This illuminates the BER performance of "Prop" outperforms those of "Ref[4]" and "RIS-OTFS-MP" under different user speeds. On the whole, the proposed method improves the BER performance of "Ref[4]" and "RIS-OTFS-MP", against the varying of the user speed v.

V. Conclusion

In this paper, we have investigated an ELM-EnCE method to improve the CE accuracy in RIS-assisted OTFS systems. Recognizing the inherent limitations of ELM, such as insufficient network parameters compared to DL networks, the paper introduces a threshold-based method to extract initial feature. This initial feature is utilized to enhance ELM learning ability, leading to an improved CE accuracy. This improved CE accuracy consequently benefits subsequent SD performance. Experimental results demonstrate that the proposed method effectively enhances SD performance and exhibits robustness against modulation order and user speed impacts.

Data availability

The datasets used and/or analysed during the current study available from the corresponding author on reasonable request.

References

1. Wang, C.-X. *et al.* On the road to 6g: Visions, requirements, key technologies, and testbeds. *IEEE Commun. Surv. Tutorials* **25**, 905–974, DOI: 10.1109/COMST.2023.3249835 (2023).
2. Hadani, R. *et al.* Orthogonal time frequency space modulation. In *2017 IEEE Wireless Communications and Networking Conference (WCNC)*, 1–6, DOI: 10.1109/WCNC.2017.7925924 (2017).
3. Raviteja, P., Phan, K. T. & Hong, Y. Embedded pilot-aided channel estimation for otfs in delay-doppler channels. *IEEE Transactions on Veh. Technol.* **68**, 4906–4917, DOI: 10.1109/TVT.2019.2906357 (2019).
4. Thaj, T. & Viterbo, E. Low complexity iterative rake decision feedback equalizer for zero-padded otfs systems. *IEEE Transactions on Veh. Technol.* **69**, 15606–15622, DOI: 10.1109/TVT.2020.3044276 (2020).
5. Wei, Z. *et al.* Orthogonal time-frequency space modulation: A promising next-generation waveform. *IEEE Wirel. Commun.* **28**, 136–144, DOI: 10.1109/MWC.001.2000408 (2021).
6. Kamble, P. & Shaikh, A. N. 6g wireless networks: Vision, requirements, applications and challenges. In *2022 5th International Conference on Advances in Science and Technology (ICAST)*, 577–581, DOI: 10.1109/ICAST55766.2022.10039549 (2022).
7. Liu, Y. *et al.* Reconfigurable intelligent surfaces: Principles and opportunities. *IEEE Commun. Surv. Tutorials* **23**, 1546–1577, DOI: 10.1109/COMST.2021.3077737 (2021).
8. Pan, C. *et al.* Reconfigurable intelligent surfaces for 6g systems: Principles, applications, and research directions. *IEEE Commun. Mag.* **59**, 14–20, DOI: 10.1109/MCOM.001.2001076 (2021).
9. Huang, C., Zappone, A., Alexandropoulos, G. C., Debbah, M. & Yuen, C. Reconfigurable intelligent surfaces for energy efficiency in wireless communication. *IEEE Transactions on Wirel. Commun.* **18**, 4157–4170, DOI: 10.1109/TWC.2019.2922609 (2019).

10. Xu, C. *et al.* Otfs-aided ris-assisted sagin systems outperform their ofdm counterparts in doubly selective high-doppler scenarios. *IEEE Internet Things J.* **10**, 682–703, DOI: 10.1109/JIOT.2022.3203895 (2023).

11. Li, Z. *et al.* Reconfigurable intelligent surface aided otfs: Transmission scheme and channel estimation. *IEEE Internet Things J.* 1–1, DOI: 10.1109/JIOT.2023.3270335 (2023).

12. Li, M., Zhang, S., Ge, Y., Gao, F. & Fan, P. Joint channel estimation and data detection for hybrid ris aided millimeter wave otfs systems. *IEEE Transactions on Commun.* **70**, 6832–6848, DOI: 10.1109/TCOMM.2022.3199019 (2022).

13. Shen, D. & Dai, L. Dimension reduced channel feedback for reconfigurable intelligent surface aided wireless communications. *IEEE Transactions on Commun.* **69**, 7748–7760, DOI: 10.1109/TCOMM.2021.3100428 (2021).

14. Xu, Y., Xie, H., Wu, Q., Huang, C. & Yuen, C. Robust max-min energy efficiency for ris-aided hetnets with distortion noises. *IEEE Transactions on Commun.* **70**, 1457–1471, DOI: 10.1109/TCOMM.2022.3141798 (2022).

15. Chen, M., Challita, U., Saad, W., Yin, C. & Debbah, M. Artificial neural networks-based machine learning for wireless networks: A tutorial. *IEEE Commun. Surv. & Tutorials* **21**, 3039–3071, DOI: 10.1109/COMST.2019.2926625 (2019).

16. Abid, M. H., Talin, I. A. & Kadir, M. I. Reconfigurable intelligent surface-aided orthogonal time frequency space and its deep learning-based signal detection. *IEEE Access* **11**, 47321–47338, DOI: 10.1109/ACCESS.2023.3273297 (2023).

17. Alzubaidi, L. *et al.* Review of deep learning: Concepts, cnn architectures, challenges, applications, future directions. *J. big Data* **8**, 1–74, DOI: 10.1186/s40537-021-00444-8 (2021).

18. Tang, J., Deng, C. & Huang, G.-B. Extreme learning machine for multilayer perceptron. *IEEE Transactions on Neural Networks Learn. Syst.* **27**, 809–821, DOI: 10.1109/TNNLS.2015.2424995 (2016).

19. Qing, C., Wang, L., Dong, L. & Wang, J. Enhanced elm based channel estimation for ris-assisted ofdm systems with insufficient cp and imperfect hardware. *IEEE Commun. Lett.* **26**, 153–157, DOI: 10.1109/LCOMM.2021.3123736 (2022).

20. Liu, J., Mei, K., Zhang, X., Ma, D. & Wei, J. Online extreme learning machine-based channel estimation and equalization for ofdm systems. *IEEE Commun. Lett.* **23**, 1276–1279, DOI: 10.1109/LCOMM.2019.2916797 (2019).

21. Carrera, D. F., Zabala-Blanco, D., Vargas-Rosales, C. & Azurdia-Meza, C. A. Extreme learning machine-based receiver for multi-user massive mimo systems. *IEEE Commun. Lett.* **25**, 484–488, DOI: 10.1109/LCOMM.2020.3031195 (2021).

22. Raviteja, P., Viterbo, E. & Hong, Y. Otfs performance on static multipath channels. *IEEE Wirel. Commun. Lett.* **10**, 745–748, DOI: 10.1109/LWC.2018.2890643 (2019).

23. Lampel, F., Avarado, A. & Willems, F. M. On otfs using the discrete zak transform. In *2022 IEEE International Conference on Communications Workshops (ICC Workshops)*, 729–734, DOI: 10.1109/ICCWorkshops53468.2022.9814589 (2022).

24. Raviteja, P., Hong, Y., Viterbo, E. & Biglieri, E. Practical pulse-shaping waveforms for reduced-cyclic-prefix otfs. *IEEE Transactions on Veh. Technol.* **68**, 957–961, DOI: 10.1109/TVT.2018.2878891 (2018).

25. Mohammed, S. K. Time-domain to delay-doppler domain conversion of otfs signals in very high mobility scenarios. *IEEE Transactions on Veh. Technol.* **70**, 6178–6183, DOI: 10.1109/TVT.2021.3071942 (2021).

26. Beixiong Zheng, R. Z. Intelligent reflecting surface-enhanced ofdm: Channel estimation and reflection optimization. *IEEE Wirel. Commun. Lett.* **9**, 518 – 522, DOI: 10.1109/LWC.2019.2961357 (2020).

27. Zhang, H., Huang, X. & Zhang, J. A. Comparison of otfs diversity performance over slow and fast fading channels. *2019 IEEE/CIC Int. Conf. on Commun. China (ICCC)* 828–833, DOI: 10.1109/ICCChina.2019.8855898 (2019).

28. Yuan, W., Li, S., Wei, Z., Yuan, J. & Ng, D. W. K. Data-aided channel estimation for otfs systems with a superimposed pilot and data transmission scheme. *IEEE Wirel. Commun. Lett.* **10**, 1954–1958, DOI: 10.1109/LWC.2021.3088836 (2021).

29. Liu, R., Huang, Y., He, D., Xu, Y. & Zhang, W. Optimizing channel estimation overhead for otfs with prior channel statistics. *2021 IEEE Wirel. Commun. Netw. Conf. (WCNC)* 1–6, DOI: 10.1109/WCNC49053.2021.9417384 (2021).

30. Liu, H., Liu, Y., Yang, M. & Zhang, Q. On the characterizations of otfs modulation over multipath rapid fading channel. *IEEE transactions on wireless communications* **22**, 2008–2021, DOI: 10.1109/TWC.2022.3208161 (2022).

31. Wang, T. *et al.* Generalized approximate message passing detector for gsm-otfs systems. *IEEE Access* **10**, 22997–23007, DOI: 10.1109/ACCESS.2022.3153703 (2022).

Acknowledgements

This work is supported in part by the National Natural Science Foundation of China (Grant No. 62301447), the Sichuan Science and Technology Program (Grant No. 2023YFG0316), the Key Scientific Research Fund of Xihua University (Grant No. Z1320929), and the Industry-University Research Innovation Fund of China University (Grant No. 2021ITA10016).

Author contributions

C.Q. conceived and designed the experiments, Z.L. and L.W. performed the experiments and collected the data, G.L. and W.H. analysed the results, C.Q. and Z.L. wrote the manuscript, X.C. and H.L. revised the manuscript critically for important intellectual content. All authors reviewed the manuscript.

Competing interests

The authors declare no competing interests.

Additional information

Correspondence and requests for materials should be addressed to C.Q.
Publisher's note Springer Nature remains neutral with regard to jurisdictional claims in published maps and institutional affiliations.